On: 24 April 2015, At: 01:42
Publisher: Taylor & Francis
Informa Ltd Registered in England and Wales Registered Number: 1072954 Registered office: Mortimer House, 37-41 Mortimer Street, London W1T 3JH, UK

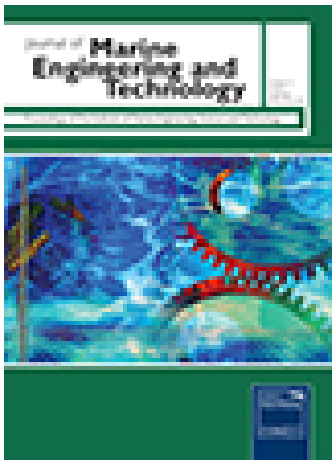

Journal of Marine Engineering & Technology

Publication details, including instructions for authors and subscription information:
http://www.tandfonline.com/loi/tmar20

Subsea cable tracking in an uncertain environment using particle filters

T. Szyrowski[a], S.K. Sharma[a], R. Sutton[a] & G.A. Kennedy[b]

[a] School of Marine Science and Engineering, Plymouth University, Plymouth, UK

[b] Camborne School of Mines, Exeter University, Cornwall Campus, Penryn, UK

Published online: 02 Apr 2015.

Journal of Marine Engineering & Technology, 2015
http://dx.doi.org/10.1080/20464177.2015.1022381

Taylor & Francis
Taylor & Francis Group

Subsea cable tracking in an uncertain environment using particle filters

T. Szyrowski[a]*, S.K. Sharma[a], R. Sutton[a] and G.A. Kennedy[b]

[a]*School of Marine Science and Engineering, Plymouth University, Plymouth, UK;* [b]*Camborne School of Mines, Exeter University, Cornwall Campus, Penryn, UK*

Localization of subsea cables is a demanding and challenging task. Among the few methods reported in the literature, magnetic field detection is the most promising one, as the cable does not require to be seen visually. Magnetic noise and a quick attenuation of the magnetic field propagating in sea water often make available methods unreliable. The authors propose a novel method of using particle filters for estimating the position of a subsea cable in a highly uncertain environment. The method was tested on data collected from a buried cable in the Baltic Sea, Denmark and shown to have a close approximation to the true location of the subsea cable. The method can be used to localize a subsea cable in an offshore noisy and uncertain environment and provides an inexpensive alternative to the use of a diver or a remotely operated platform.

Introduction

Subsea cables play an important role in current economy. They provide power and communications links between continents and islands, and also connect a growing number of offshore installations. The subsea cables need to be periodically checked, localized and repaired for faults. Localization of the subsea cables is a difficult and costly task, as dynamic sea environments keep changing the cables' initial position and their burial depth (Szyrowski et al. 2013a).

The current state of knowledge in estimating position and burial depth of marine power cables relies on a mainly deterministic approach and mathematical inversion methods (Cowls & Jordan 2002; Won 2003; Szyrowski et al. 2013b). A magnetic signal emitted from the cable is sampled in two different points in space and attenuates at a faster rate because of the salinity of sea water. The magnetic field signal can thus be measured only in close proximity from the source, and in practice the signal can only be measured within a 5 m range (Takagi et al. 1996; Kojima et al. 1997; Szyrowski et al. 2013b). This creates a problem in marine survey, as it has to be performed by a remotely operated vehicle or a specialized driver and thus susceptible to increases in operational cost and risks to human health and life. The diver can only remain in the water for a short period of time, and it is difficult to operate in limited visibility and/or strong currents. In addition, the localization of the cable based on a human's judgement is susceptible to errors and not reliable in most cases (Ortiz et al. 2000).

One solution to this is to devise a surveying method from the surface of the sea without engaging a diver. This will require a reliable method for long-range detection, which can cope with the uncertain environment to reduce the effects of noises coming from various sources such as engines of the surveying boat, communication devices and other sources of magnetic fields.

This paper introduces a novel stochastic method based on particle filters to estimate the distribution of a magnetic field on the sea surface in an uncertain environment and accurately predict the location of the cable. Following on from this introductory section, the rest of the sections are summarized as follows. The underlying magnetic field emitted from a conducting wire and the current localization methods is investigated. Then, the model of the magnetic field distribution from a subsea cable is described, followed by a a general background of particle filtering and its application to the localization of subsea cables. The paper finishes with concluding remarks.

Magnetic-field distribution from a very-low-frequency current-carrying conductor

The magnetic and electric fields surrounding a submarine cable originate from the electric currents and charges that either exist in the cable or are induced in surrounding waters. The fields can be determined by solving Maxwell's equations (Olsen & Wong 1992). The magnetic field from a distribution of current at any point in space can be determined by the formula:

$$\boldsymbol{B} = \nabla \times \int_{\text{All space}} \frac{\mu_0 \boldsymbol{J}(t - (r/c))}{4\pi r} \, \mathrm{d}v \qquad (1)$$

where $\boldsymbol{B}$ is the magnetic flux density, c is the speed of light, $\boldsymbol{J}$ is the distribution of the current in space, r is the distance

*Corresponding author. Email: tomasz.szyrowski@plymouth.ac.uk

from the source to the field point, μ_0 is the permeability of free space, and $\nabla\times$ is the curl operator.

For the purpose of a submarine cable survey, the frequency of the time-varying current is often in the range of 25–100 Hz. Use of these extremely low frequencies (ELF) is mainly determined by the relation between the frequency and attenuation of the magnetic field in sea water (Szyrowski et al. 2013b). The use of ELF allows a quasi-static approach to the analysis of the magnetic field where the spatial distribution of the field maintains the same shape, but its amplitude varies in time with the source. The same does not necessary hold for a high-frequencies method (Olsen & Wong 1992).

Olsen and Wong (1992) proposed that a magnetic field (MF) can be described by three components. A 'static' MF is characterized by the term $(1/r^3)$, an 'induction' component by $(1/r^2)$ and a 'radiation' term by $(1/r)$. In the quasi-static method, the effect of the radiation field is neglected, as the ratio of the contribution from the radiation field to the static field in the MF is very small (Olsen & Wong 1992).

A submarine cable can be modelled as an infinitely long current-carrying wire. The MF from cable is calculated using Equation (2) below by adding the MF from the individual dipoles placed along the z-axis (Olsen & Wong 1992).

$$\boldsymbol{B} = \frac{\mu_0\, I\, a^2}{4\pi} \left\{ \int_{-\infty}^{\infty} \frac{I(z')\cos[\omega t - k(\rho^2 + (z-z')^2)^{1/2}]\rho\ \mathrm{d}z'}{(\rho^2 + (z-z')^2)^{3/2}} - \int_{-\infty}^{\infty} \frac{k\, I(z')\sin[\omega t - k(\rho^2 + (z-z')^2)^{1/2}]\rho\ \mathrm{d}z'}{\rho^2 + (z-z')^2} \right\} \tag{2}$$

where $I(z')$ is the current along the z-axis, $\rho = (x^2 + y^2)^{1/2}$ and $\sin\theta = \rho/r$.

Equation (2) is difficult to solve, and the MF from a uniform current $I(t)$ along an infinitely long wire can be solved easily using Ampere's law, since, in a quasi-static mode, the current shape can be assumed constant in space with only amplitude varying in time:

$$\boldsymbol{I}(t) = I\cos(\omega t) \tag{3}$$

For an electric current density $\boldsymbol{J}$ and circle of radius C centred on the wire, with the surface S, which includes the wire, Ampere's law in its integral form is given by:

$$\int_C \boldsymbol{B}\cdot \mathrm{d}l = \mu_0 \int_S (\boldsymbol{J} + j\,\omega\,\epsilon_0\,\boldsymbol{E})\cdot \mathrm{d}\boldsymbol{s} \tag{4}$$

The left-hand side of Equation (4) is equal to $2\,\pi\rho B_\Phi$, and the other components of the MF are zero. On the right-hand side, the integral gives the total current on the wire ($I\cos(\omega t)$). Olsen and Wong (1992) argue that for very slow time-varying fields, the magnetic and electric fields become uncoupled and independent of each other, and the term $[j\,\omega\,\epsilon_0\,\boldsymbol{E}]$ can be ignored.

The MF density resulting from the current I flowing through the straight conductor with the length $\overrightarrow{\mathrm{d}l}$ can be calculated using the Biot–Savart law (Dezelak et al. 2010):

$$\boldsymbol{B} = \frac{\mu_0\, I}{4\pi\ r}\,(\overrightarrow{dl}\ \times\ \vec{r}) \tag{5}$$

This approach can be problematic if the conductor does not follow a straight path. The problem of the different geometry of the carrying current wire was considered by Olsen et al. (1988). They proposed approximating the current path by straight line segments with a constant current. The MF at sample point P can be described by the equation:

$$\boldsymbol{B}_P = \mu_0 \sum_{i=1}^{N} \frac{I_i}{4\pi\ |r_{iP}|}\,(\sin\theta_{i1} + \sin\theta_{i2})\ a_i\ \times\ a_{iP} \tag{6}$$

where N is the number of segments, I_i is the current on segment i, $|r_{iP}|$ is the length of the vector from the centre of segment i to point P, a_i is a unit vector in the direction of segment i, and a_{iP} is a unit vector in the direction of vector r_{iP}.

The analytical solution for the MF from a single current-carrying conductor can be obtained using the 3-D Integration Technique (El Dein 2009) based on the Biot–Savart law as:

$$\boldsymbol{B}_P = \mu_0 \int_l \frac{\vec{I}(l)\ \mathrm{d}l\ \times\ \overrightarrow{a_P}\ (l)}{4\pi\ |\overrightarrow{r_P}\ (l)|^2} \tag{7}$$

where l is the parametric position along the current path, $\vec{I}(l)$ is a line current, $\overrightarrow{r_P}(l)$ is a vector from the source point $S = (x_s, y_s, z_s)$ to the field point $P = (x_P, y_P, z_P)$, $\overrightarrow{a_P}$ is a unit vector in the direction of $\overrightarrow{r_P}\ (l)$, and $\mathrm{d}l$ is a differential element in the direction of the current.

The calculation of the MF from the overhead transmission lines assumes that the line is surrounded by air with zero or negligible conductivity. This is not the case if the line is buried in the soil or submerged in saltwater. Gard (2002) considered the MF for buried cables, where the conductivity and permittivity are different from that in the air. He considered the cable as straight sections of line where the magnetic flux is radially symmetric and can be considered to resemble cylindrical shells. The magnetic flux density could then be described by:

$$\vec{\boldsymbol{B}} = \frac{\mu_r\,\mu_0\, I}{2\pi\, r}\,\overrightarrow{\alpha_\phi} \tag{8}$$

where $\overrightarrow{\alpha_\phi}$ is the tangential unit vector in a cylindrical coordinate system, and μ_r is the relative permeability of the soil.

Equation (8) can be translated to Cartesian coordinate as:

$$\vec{B} = \frac{-\mu_r \mu_0 I(y+d)}{2\pi\ (x^2+[y+d]^2)}\ \overrightarrow{\alpha_x} + \frac{-\mu_r \mu_0 Ix}{2\pi\ (x^2+[y+d]^2)}\ \overrightarrow{\alpha_y} \quad (9)$$

The propagation of an MF in sea water involves many difficulties and has been a topic of research for many years. It is mostly affected by four properties of the sea (Bogie 1972). One of these factors is conductivity, with a typical value of 4 Siemens per metre (S/m) for sea water and 0.001 S/m for freshwater (King 1989). Conductivity depends upon factors such as salinity, temperature, and pressure or excitation frequency. The second is permeability, which is usually taken as its value for free space ($4\pi\ 10^{-7}$ Henrys/m). The permeability for non-ferromagnetic media such as sea and freshwater can be negligible. The third is permittivity and is correlated with frequency but for polar liquids can be considered constant for frequencies below 10^9 Hz. The permittivity of free space varies between $78\ \times\ 10^{-13}$ and $81\ \times\ 10^{-13}$ Farads/m. The fourth factor is polarization. Sea water is an electrolyte, and unless the flowing current is alternating, the polarization has an impact on the magnetic propagation.

A comparison of the attenuation in different types of water was conducted by Abdou et al. (2011). The authors point out that the complex propagation constant γ is described by an attenuation constant $\propto$ and phase constant β as in Equation (10):

$$\gamma = \alpha + j\,\beta \quad (10)$$

All the calculations were assumed on the basis that the current is carried by an infinitely thin wire. For the purpose of marine surveys, the thickness of the cable can be neglected. The distance between the cable and the sea surface often exceeds 3 m, which is dictated by the safe depth of a marine survey boat operation, and the thickness of the modern submarine cable is 0.069 m. It is safe to assume that the distance is measured from the centre of the cable.

Current methods for subsea cable detection and tracking use a deterministic source estimation based on a single sample point (Szyrowski et al. 2013b). The measurement is taken in a single location, and the distance calculated is based on a difference of the coils readings. The main assumption is that the strength of the MF at a sample point from the source can be fully described by a distance from the source and with a simple decay function. Cowls and Jordan (2002) have pointed out that this assumption is not always true. They used a linearization algorithm to calculate signal-strength decay in relation to the distance x from the source. They suggested that signal strength decays with a factor of x^{-3}. The decay of magnetic signals is also considered by Al-Shamma'a et al. (2004). They proposed that the conductivity of the sea water was the main reason for MF attenuation. They suggested that the attenuation of the magnetic signal strength E increases with distance and follows Maxwell's equation: $E = E_0\, e^{(-\alpha\, x)}$, where x is the distance between the transmitter of a magnetic signal and the receiver, and α is the attenuation factor measured in decibels per metre (dB/m).

One of the existing methods for a cable localization is a Tinsley MKII cable detector (Tinsley 2012). The operating principles of the Tinsley method are based on the

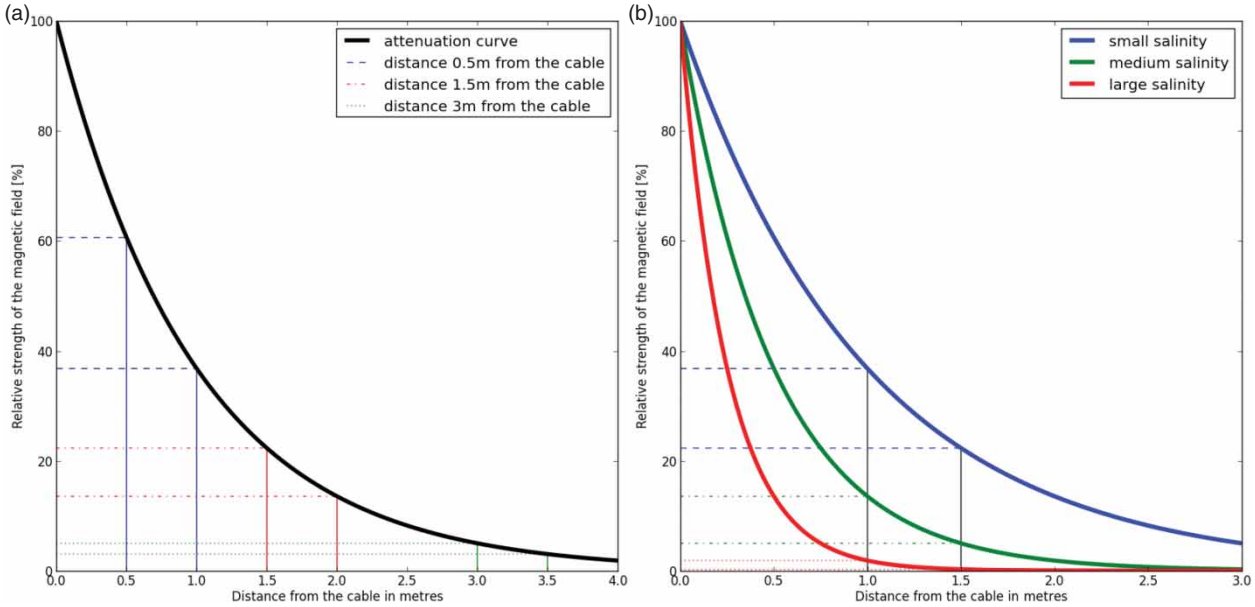

Figure 1. Difference in the coil's readings for (a) different distances from the cable and (b) a MF attenuations in sea water.

assumption that the MF attenuation in sea water can be described by an exponential decay curve. The signal from the source is sampled by two horizontal coils placed 0.5 m from each other. The difference in readings compared with the decay curve gives an estimation of the distance between the coils and the cable.

Figure 1(a) illustrates the sampling on the decay curve. The dashed lines correspond to the readings from the pair of horizontal coils when the frame is placed at a distance of 1 m, 1.5 m and 3 m, respectively. Given that the attenuation rate related to salinity is known, the difference between the coil's readings can be referenced to the distance from the source.

The attenuation curve is not a general characteristic for sea water. It largely depends on the salinity and related to the conductivity of the water. An estimated relation between water salinity and coils readings is illustrated in Figure 1(b). It should be noted that the salinity of the water and its impact on the MF attenuation can only be approximated by the exponential curve. In the marine environment, the conductivity of the water can have different layers and can change over time.

The estimation of the distance based on the difference between coil readings limits the Tinsley method to 3 m from the cable. This limitation comes not only from MF attenuation; primarily after the 3 m range, the difference becomes very small and estimation is ambiguous.

Modelling of MF emanating from the subsea cable

To investigate the propagation of the MF from a wire buried in the sea bed, theoretical modelling was conducted first. For the purpose of a basic search algorithm, a simple model is implemented.

The most basic model consists of the cable's line following a given equation. The induced MF on the water surface is represented by a vector field on the plane $z = 0$. The MF from the cable is approximated as a function of its current, the shortest distance from the cable, a single attenuation parameter and a flux vector as a cross-product of the cable's tangent vector and the shortest distance vector.

The MF is sampled along the path covered by a survey platform with mounted magnetic sensors. The samples are taken at equal time intervals at a constant speed with the platform moving along the lines perpendicular to the cable's direction. The path of the platform can be modelled by a sinusoidal function and can be called a sensor's path. The MF on the water surface constitutes a mesh, which can be interpolated to any point along the sensor's path. The mesh is constructed from a finite number of points, and the shortest distance to the cable is calculated from each point. The direction of the MF will be given by the direction of the unit vector, which is the cross-product of the direction of the cable and that of the shortest distance. The magnitude of the MF will be calculated from the distance and the attenuation factor.

The MF resulting from the current in the cable is sampled with magnetic sensors. A good description of sensors based on inductance coil can be found in Tumanski (2007). The transfer function $V = f(\boldsymbol{B})$ describes a coil's output voltage V as a signal related to changing MF $\boldsymbol{B}$ and is defined by Faraday's law of induction:

$$V = -n\frac{\mathrm{d}\phi}{\mathrm{d}t} = -n\,A\frac{\mathrm{d}\boldsymbol{B}}{\mathrm{d}t} = \mu_0\, nA\frac{\mathrm{d}H}{\mathrm{d}t} \tag{11}$$

In Equation (11), ϕ is the magnetic flux through a coil with n turns and area A. The signal from the coil V is proportional to the rate of change in flux density $\mathrm{d}\boldsymbol{B}/\mathrm{d}t$ and requires integration of the coil output over the time of phase or full cycle of an alternating MF.

To verify the theoretical aspects of this work, data were collected during a real survey in the Baltic Sea. The searching coils were on board of the survey platform, which was an 8 m boat. The horizontal coil was placed aligned with the boat heading, and the vertical coil was placed in the direction of the vector $[x,y,z] = [0,0,1]$.

The vectors of the platform's heading and MF are shown in Figure 2. All three components of the MF source change with the movement of the platform. As the platform moves from point P_{k-1} to P_k by a vector $\boldsymbol{p}_k(p_k^{(x)}, p_k^{(y)}, p_k^{(z)} = 0)$, the dominating source of the MF moves by the projection of the vector $\boldsymbol{p}_k$ into the vector of the direction of the cable $\boldsymbol{d}_k(d_k^{(x)}, d_k^{(y)}, d_k^{(z)})$. The vector $\boldsymbol{d}_k$ is the vector of the cable at the source S_k. A moving charge of electric current moves on the same path, and so the vector $\boldsymbol{d}_k$ is also in the direction of the moving charge.

During the survey, the position of the survey boat is read by a precise global positioning system (GPS) reading, and a tidal height variations control system was used to correct the measurement of the water column depth.

The strength of the MF above the cable can be described as a distribution with a given shape as shown in Figure 3. Each sample point can be represented as the column vector of the position's components P_k, but it also needs to incorporate the vector direction of the cable $\boldsymbol{d}_k$ at the time step k and a vector of platform heading $\hat{\boldsymbol{h}}_k$, which in practice gives an orientation of the sensors. As the future direction of the cable can be only assumed based on the past data, the direction of the cable at the source point S_k can be estimated as $\hat{\boldsymbol{d}}_k$ where the hat notation represents the unit vector.

$$x_k = \begin{bmatrix} P_k \\ \hat{\boldsymbol{h}}_k \\ \hat{\boldsymbol{d}}_k \\ S_k \end{bmatrix} \tag{12}$$

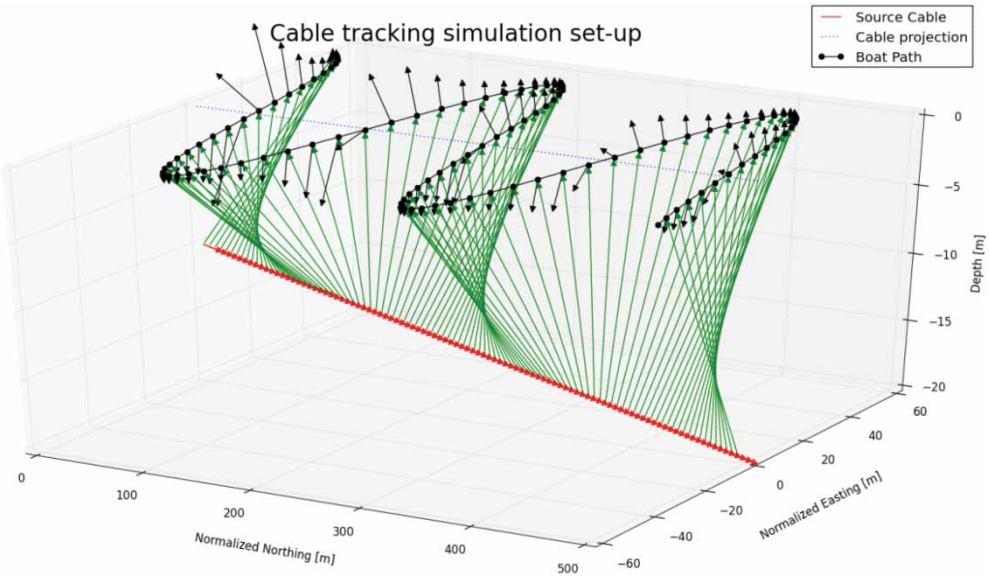

Figure 2. Visualization of vector directions.

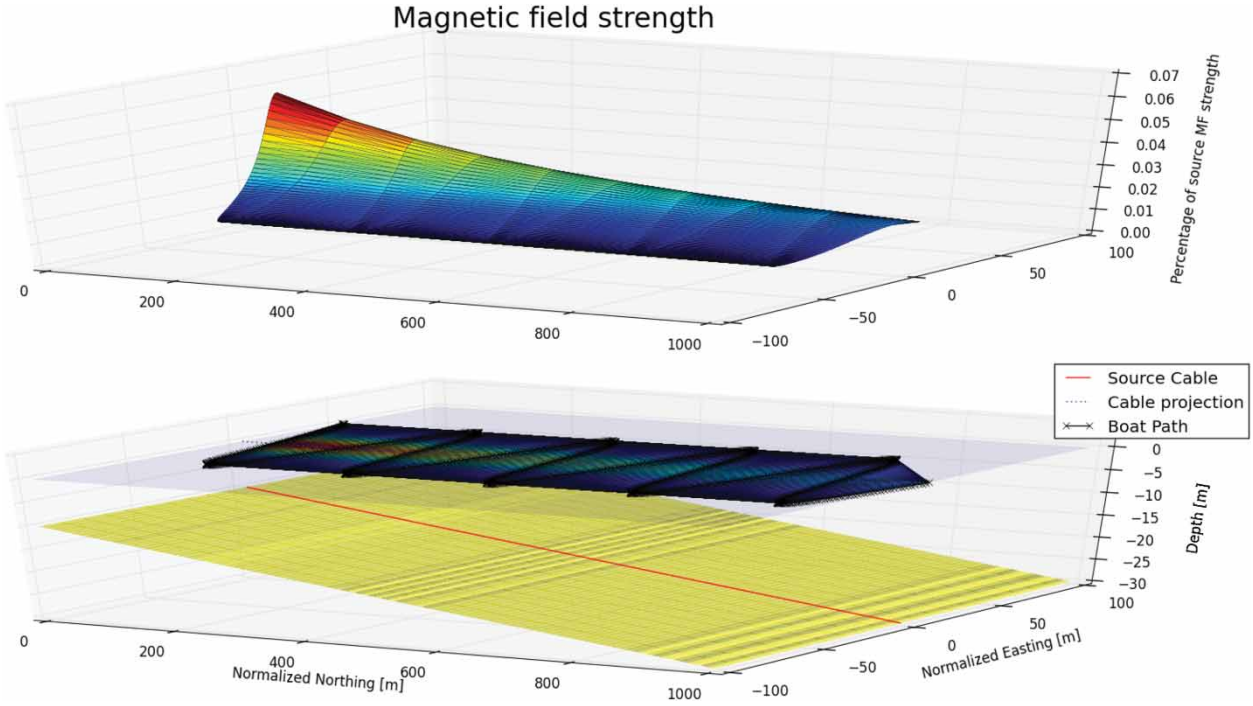

Figure 3. Strength of MF above the cable.

The MF distribution can be described as integration along all sample points.

$$\int_{k=1}^{k=n} f\,(x_k) \;+ wh_k + \; wp_k + \; wd_k = \int_{k=1}^{k=n} \begin{bmatrix} P_k + wP_k \\ f_h(\hat{\boldsymbol{h}}_{k-1}) + \; wh_k \\ f_d(S_{k-1},\;\; S_k) + \; wd_k \\ S_{k-1} + (\boldsymbol{p}_k \cdot d_k)\hat{\boldsymbol{d}}_k + \; wP_k \end{bmatrix} \tag{13}$$

The noise wP_k relates to estimation of the position of the source point along the direction of the cable. This noise comes from readings of the platform's position and can be assumed to be white Gaussian. Similarly the noise of the sensor's heading wh_k comes from sensor inaccuracies and from the survey platform's pitch, roll and yaw. The noise can also be assumed to be a white Gaussian.

If the cable follows a bent curve, while a small range the path can be approximated by a second-order fit. In such cases, the function $f_d(S_{k-1},\;\; S_k)$ can become a nonlinear

regression or spline and can incorporate n source points to become $f_d(S_{k-n}, S_{k-n+1}, \ldots, S_k)$. The noise wd_k will follow a deviation from the straight line and will not be white Gaussian.

The MF $\boldsymbol{B}_k$ at the measurement point P_k can be calculated based on the Biot–Savart law as described in Equations (7), (8) and (9), and can be simplified as:

$$\boldsymbol{B}_k = \frac{\mu_0 I}{4\pi\ r_k^3}(\ \hat{\boldsymbol{d}}_{k+1}\ \times\ \boldsymbol{r}_k) = \frac{\mu_0 I}{4\pi\ r_k^3}\ (\hat{\boldsymbol{d}}_{k+1} \times [P_k - S_k]) = c\frac{(\ \widehat{\boldsymbol{d}}_{k+1} \times [P_k - S_k])}{r_k^3} \tag{14}$$

In Equation (14), $\mu_0 I/4\pi$ is constant along the cable and can be written as a constant c.

The state equation allows us to calculate the MF vector $\boldsymbol{B}_k$ pointing from the measurement point P_k.The MF at the point is measured by two coils. One of the coils is placed horizontally in the direction of the platform path. The second coil is placed vertically to the water's surface. This set-up is depicted in Figure 4.

The measurement model can be defined as the output from the coils placed in the MF with vector $\boldsymbol{B}$ as described in Equation (11).

Figure 5 shows theoretical readings from both horizontal and vertical coils. The left part of the figure represents the horizontal coil's output with a single peak above the cable. The right part of the figure represents the vertical coil's output. The vertical coil outputs a zero voltage above the cable with two peaks on both sides of the cable.

It must be noted that the MF is orthogonal to the cable's vector direction $\boldsymbol{d}_k$ and the vector $\boldsymbol{r}_k$ pointing form the source point S_k to the sample point P_k.

The measurement equation depends upon the sensors and, in the case of two searching coils, can be described as:

$$z_k = h(x_k) + \ v_k = \begin{bmatrix} C_H + v_k^H \\ C_V + v_k^V \end{bmatrix} = \begin{bmatrix} \boldsymbol{B}_k \cdot \hat{\boldsymbol{h}}_k\ + v_k^H \\ \boldsymbol{B}_k \cdot \hat{\boldsymbol{z}}\ + \boldsymbol{v}_k^V \end{bmatrix} \tag{15}$$

In Equation (15), value $C_H + v_k^H$ is the output from the horizontal coil where v_k^H is the measurement noise and likewise $C_V + v_k^V$) the output from the vertical coil with v_k^V representing the measurement noise. The vector $\hat{\boldsymbol{p}}_k$ is a unit vector of the boat movement assuming that the centre line of the horizontal coil is placed in the same direction as the vector $\boldsymbol{p}_k$. The vector $\hat{z} = [0, 0, 1]$ is a unit vector in the z-direction and direction of the vertical coil. In other words, the measurement of the coil is the result of the projection of the MF along the direction of the coil's centre line.

The measurement noise v_k is related to the output of the coils, precision of the hardware and surrounding magnetic noises. It can be assumed that this is white Gaussian noise.

Thus, combining Equations (14) and (15) gives the measurement function in terms of state variables:

$$z_k = \begin{bmatrix} c\dfrac{(\ \hat{\boldsymbol{d}}_{k+1}\ \times\ [P_k - S_k])}{|[P_k - S_k]|^3} \cdot\ \hat{\boldsymbol{h}}_k\ + \boldsymbol{v}_k^H \\ c\dfrac{(\ \hat{\boldsymbol{d}}_{k+1} \times [P_k - S_k])}{|[P_k - S_k]|^3} \cdot [0, 0, 1]\ + \boldsymbol{v}_k^V \end{bmatrix} \tag{16}$$

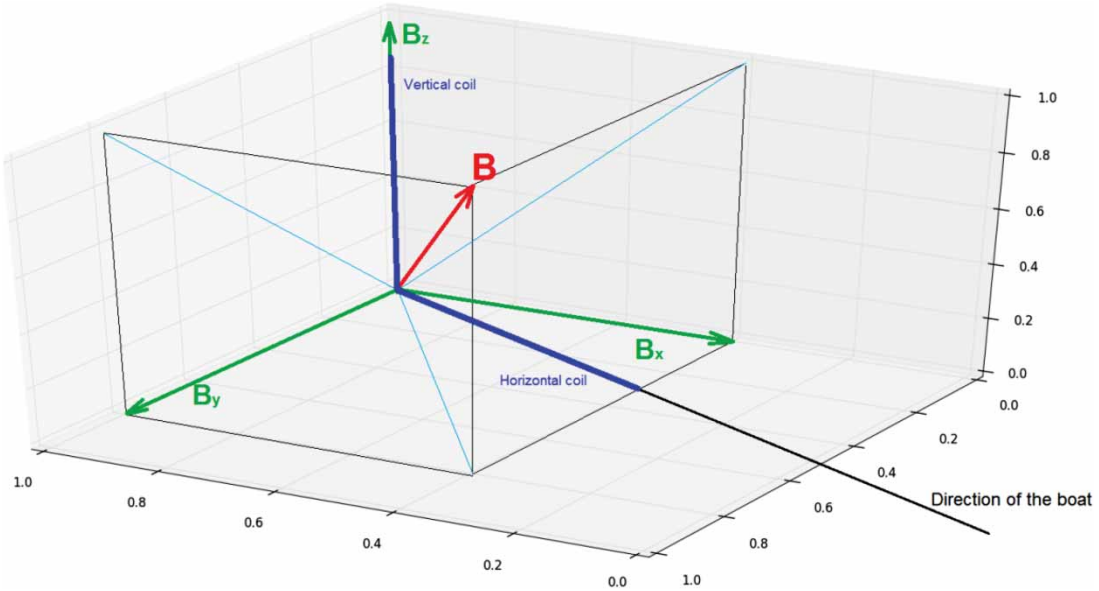

Figure 4. Direction of measurement coils in relation to the vector of MF.

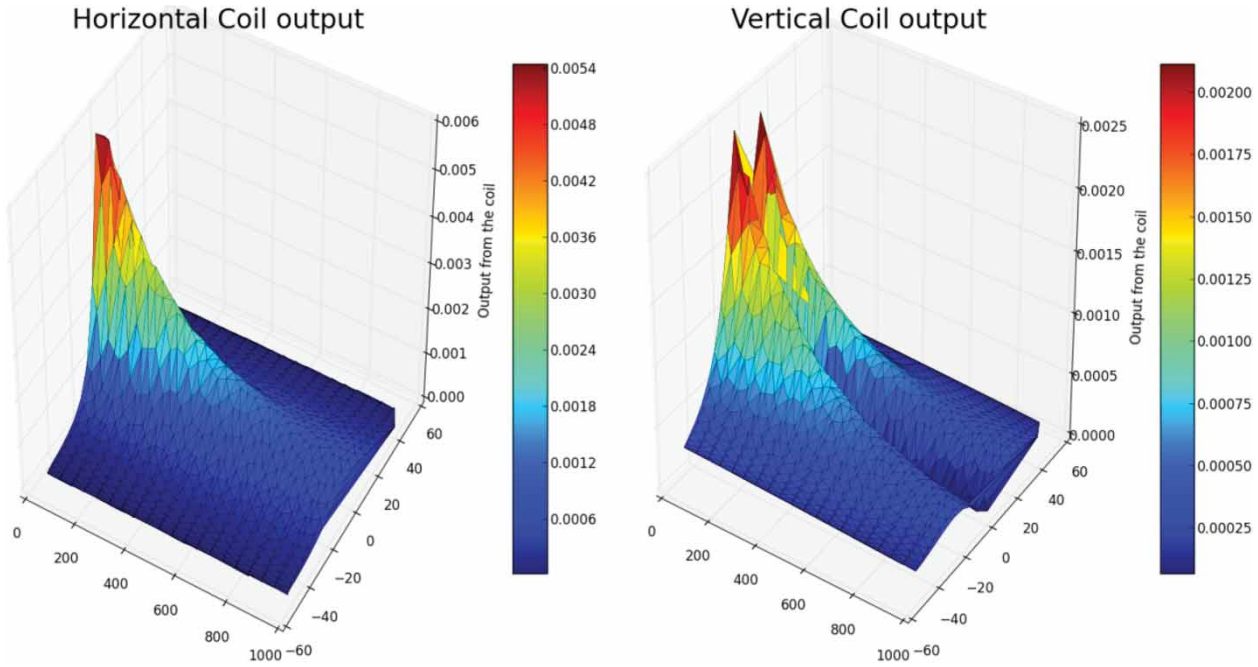

Figure 5. Distribution of readings from horizontal and vertical coils.

Equation (16) can be represented as the Cartesian components of the vectors:

$$z_k = \begin{bmatrix} \dfrac{c}{|[P_k - S_k]|^3} \begin{bmatrix} \hat{x} & \hat{y} & \hat{z} \\ \hat{d}_{k+1}^{(x)} & \hat{d}_{k+1}^{(y)} & \hat{d}_{k+1}^{(z)} \\ P_k^{(x)} - S_k^{(x)} & P_k^{(y)} - S_k^{(y)} & P_k^{(z)} - S_k^{(z)} \end{bmatrix} \cdot \begin{bmatrix} h_k^{(x)} \\ h_k^{(y)} \\ h_k^{(z)} \end{bmatrix} + v_k^H \\ \dfrac{c}{|[P_k - S_k]|^3} \begin{bmatrix} \hat{x} & \hat{y} & \hat{z} \\ \hat{d}_{k+1}^{(x)} & \hat{d}_{k+1}^{(y)} & \hat{d}_{k+1}^{(z)} \\ P_k^{(x)} - S_k^{(x)} & P_k^{(y)} - S_k^{(y)} & P_k^{(z)} - S_k^{(z)} \end{bmatrix} \cdot \begin{bmatrix} 0 \\ 0 \\ 1 \end{bmatrix} + v_k^V \end{bmatrix} \tag{17}$$

where, in Equation (17), the vector product can be expanded as:

$$\begin{aligned} &\begin{bmatrix} \hat{x} & \hat{y} & \hat{z} \\ \hat{d}_{k+1}^{(x)} & \hat{d}_{k+1}^{(y)} & \hat{d}_{k+1}^{(z)} \\ P_k^{(x)} - S_k^{(x)} & P_k^{(y)} - S_k^{(y)} & P_k^{(z)} - S_k^{(z)} \end{bmatrix} \\ &= (\hat{d}_{k+1}^{(y)}(P_k^{(z)} - S_k^{(z)}) - \hat{d}_{k+1}^{(z)}(P_k^{(y)} - S_k^{(y)}))\hat{x} \\ &\quad + (\hat{d}_{k+1}^{(x)}(P_k^{(z)} - S_k^{(z)}) - \hat{d}_{k+1}^{(z)}(P_k^{(x)} - S_k^{(x)}))\hat{y} \\ &\quad + (\hat{d}_{k+1}^{(x)}(P_k^{(y)} - S_k^{(y)}) - \hat{d}_{k+1}^{(y)}(P_k^{(x)} - S_k^{(x)}))\hat{\boldsymbol{z}} \end{aligned} \tag{18}$$

Using the fact that the vertical coil output is a dot product of unit $\hat{\boldsymbol{z}}$ vector, Equation (17) can be simplified to:

$$z_k = \begin{bmatrix} \dfrac{c}{|[P_k - S_k]|^3} \begin{bmatrix} \hat{x} & \hat{y} & \hat{z} \\ \hat{d}_{k+1}^{(x)} & \hat{d}_{k+1}^{(y)} & \hat{d}_{k+1}^{(z)} \\ P_k^{(x)} - S_k^{(x)} & P_k^{(y)} - S_k^{(y)} & P_k^{(z)} - S_k^{(z)} \end{bmatrix} \cdot \begin{bmatrix} h_k^{(x)} \\ h_k^{(y)} \\ h_k^{(z)} \end{bmatrix} + v_k^H \\ \dfrac{c}{|[P_k - S_k]|^3} (\hat{z} + \hat{d}_k^{(z)} + (P_k^{(x)} - S_k^{(x)})) + v_k^V \end{bmatrix} \tag{19}$$

where, in Equation (19), the term $|[P_k - S_k]|$ is the length of the distance vector r_k from the source to the measurement point. The modulus is defined as follows:

$$\begin{aligned} &|[P_k - S_k]| \\ &= \left(\sqrt{(P_k^{(x)} - S_k^{(x)})^2 + (P_k^{(y)} - S_k^{(y)})^2 + (P_k^{(z)} - S_k^{(z)})^2} \right) \end{aligned} \tag{20}$$

In the case when the survey platform moves along the path perpendicular to the direction of the cable, Equation (15) reduces to trigonometric functions with sine and cosine of the MF strength:

$$z_k = \begin{bmatrix} \cos(|\boldsymbol{B}_k|) + v_k^H \\ \sin(|\boldsymbol{B}_k|) + v_k^V \end{bmatrix} \tag{21}$$

This simplified relation in Equation (21) will be used in the implementation of a particle filter where the boat path can be assumed to be a straight line perpendicular to the cable. In that case, the magnetic source can be assumed as a point resulting from a cross-section of the cable.

The configuration of the coils and placing the horizontal coil axis in line with the platform's heading ensures the best readings from the horizontal coil are obtained. An offset from the path perpendicular to the cable results in corrupted readings. The corruption in the readings can be calculated by the sine of an angle between the platform's direction and the cable direction. For a small offset such as yaw and roll, it is assumed to be a white noise. The perpendicular platform's path ensures the best possible readings and signal-to-noise ratio.

Particle filters for estimation of cable location

The position and direction of the cable here will be estimated using particle filters techniques, a stochastic approach. Particle filters were introduced by Gordon (1993) as a robust Bayesian approach to estimate dynamical state probability density functions (PDF) (Fallon and Godsill 2010; Crisan & Obanubi 2012). The need to construct such a filter arose from a consideration of nonlinear or non-Gaussian problems without a general analytic expression for the required PDF. The main idea behind particle filters is to approximate recursively the PDF by a set of random samples called particles. The particles tend to concentrate in the regions of high probability density and hence give an approximation of the true PDF value.

The particle filter algorithm propagates and updates a set of random samples $\{x_{k-1}(i) : i = 1, \ldots, N\}$ from the PDF $p(x_{k-1}|D_{k-1})$ to obtain a set of values $\{x_k(i) : i = 1, \ldots, N\}$ with a distribution close to $p(x_k|D_k)$.

A schematic representation of the particle filter algorithm is represented in Figure 6. At every iteration, a set of particles is initialized. This set constitutes an N-number of theoretical sources. For every particle's

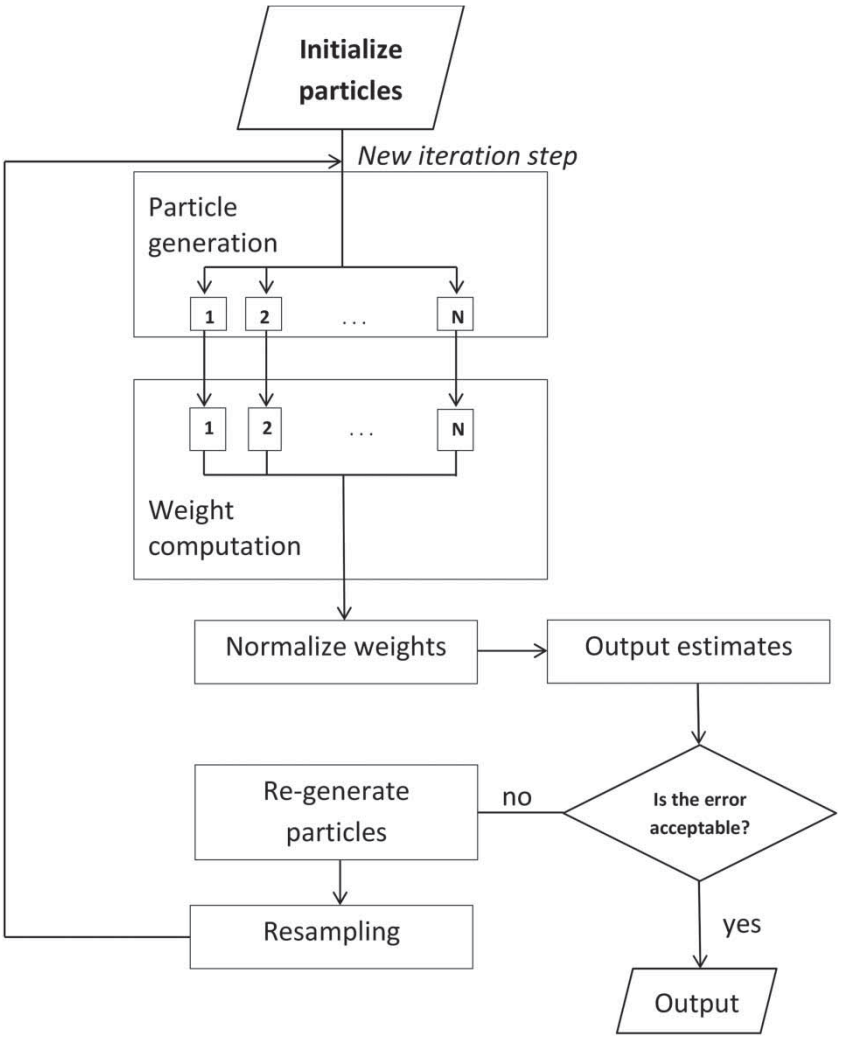

Figure 6. Particle filter algorithm.

source, the calculated theoretical MF produces the distribution of horizontal and vertical coil's readings at each sample point. The distributions of the readings are compared with experimental data. The sum of absolute distances between theoretical readings and measured readings at each point gives the overall difference between the theoretical and measured distribution. The inverse of the overall distance is assigned to each particle as a weight. The weights are normalized to sum up to unity.

From the set of particles, the particle with the highest weight is the most plausible for the true cable's location. The rest of the particles in the set tend to cumulate around the best solution. The spread of the particles gives a tolerance to the true localization. If the tolerance is larger than the accepted solution, the particles are regenerated and resampled.

In the regeneration step, only a quartile of particles with the highest weights are chosen. To test different solutions, for each chosen particle, three new particles are randomly generated. The particles diverge from the initial one, inversely proportional to its weight. If the weight of the initial particle is high, the new particles test solutions in a small proximity to the initial source. If the weight of the particle is low, the new particles test a wider range of possible solutions.

After the regeneration step, the algorithm starts a new iteration, where, for each particle, the MF and the resulting theoretical coil readings are generated, and the weights are computed.

Results and discussion

The main purpose of the cable survey is to estimate its exact location in terms of a geographical position and its burial depth. The geographical position can be expressed as GPS readings or as a coordinates in a local grid. The most common GPS positioning for underwater surveys has serious limitations. The reading is not possible underwater and is always related to the surface reading. Knowing the GPS position of the surveying platform and taking it as a centre of the coordinates system helps simplify the cable survey.

The burial depth can also be related to the platform position. A water depth echo sounding is standard practice during a marine survey. Calculation of the burial depth is a straightforward difference between the length of the water column below the samples and the distance from the cable.

All positioning parameters can be estimated using a particle filter. To confirm the method, an experiment was conducted near the Danish shore on the Baltic Sea. The cable was partially buried in a sandy sea bed. A very-low-frequency alternating current was induced in the armour of the power cable, and the MF was sampled on the sea surface, where the water depth was 4–15 m. During the experiment, samples were taken every second. With the boat moving at 3–4 knots, the distance between points was approximately 2 m.

Particle filtering for point localization

Initially, a particle filter was used to establish the region of interest (ROI) from the readings of both vertical and horizontal coils. The reading from the horizontal coil is related to the signal's MF through the cosine function. This means that the output from the horizontal coil reaches its peak above the cable. The reading from the vertical coil is related by the sine function, and the reading directly above the cable would give a zero reading. The ROI is calculated as the square area below the sample point with a maximum distance between the horizontal and vertical coils. The sample is not necessarily taken above the cable, and the reading is corrupted by noise. For this reason, the ROI is extended to cover 20 sample points before and 20 sample points after the initial source. For each sample point, the depth of the water column is measured by an echo sounder. The cable can lie on the sea bottom, buried up to 3 m or suspended in the water. The height of the ROI is taken from 3 m below the sea floor to 2 m above.

Each particle represents a hypothetical source. For calculating the distribution of the MF, not only the position of the source but also its attenuation is important. The attenuation is related to the water conductivity whose general value is known before the survey. The conductivity of the sea water varies from about 1 S/m in the Baltic Sea to 5 S/m in the sea around the UK. The estimated value for the survey area was 1.6 S/m. Each particle in the ROI has a randomly assigned conductivity that is bound by 0.5 S/m below and above the estimated value.

The results from the particle filter are compared with an output from a traditional inspection method where the diver localizes the cable using a proprietary technique based on the Tinelsey 5930 MK II (Tinsley 2012).

In an initialization step, N particles are drawn. The number of particles is arbitrarily chosen as $N = 1000$. For each particle, the theoretical distribution of the MF is calculated. From this distribution, the theoretical readings of the horizontal and vertical coils are calculated for each data point.

Figure 7 shows the initialization of a particle filter. The left image shows the ROI and 1000 hypothetical sources. The line with a $\times$ symbol represents the horizontal coil readings for each sample point, and the line with a $+$ symbol represents the vertical coil readings.

After the particles' initialization, particle weights are assigned to each theoretical source. The square root distances between the experimental and calculated coil readings are normalized and assigned to particles. A particle's probability of being chosen depends upon its weight and is higher if the distance between the particle distribution and the experimental readings is shorter.

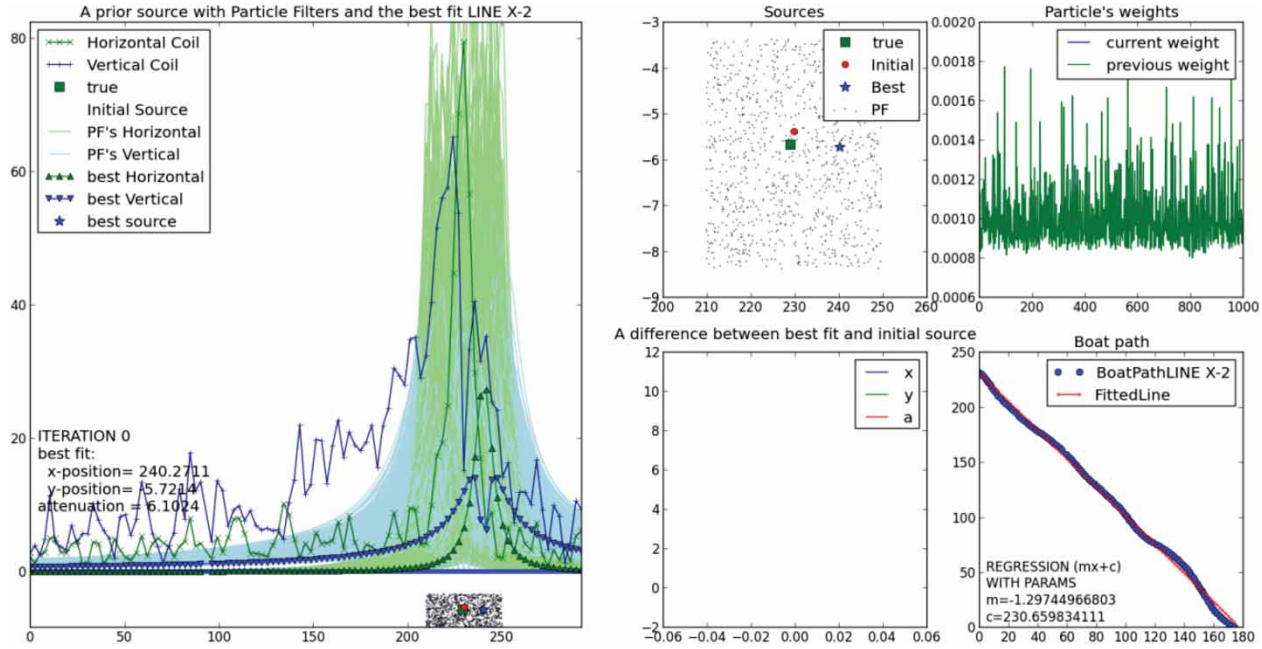

Figure 7. Initialization of particle filter.

New theoretical sources are included in the next step after resampling the area, and the particle weights are recalculated. Gaussian noise is added to the position, and an attenuation parameter is assigned to each particle. The noise depends upon the particle weight. The greater weight comes from the particle with a smaller distance, thus closer to the real source. If the weight of the particle is greater, the added noise is smaller to test an area in close proximity to the particle. Figure 8 shows a conversion of sources after 10 iterations. The hypothetical sources concentrate in the region of most acceptable area near the true source. In Figure 8, the star point represents the source with the shortest distance from the experimental readings. The distributions of theoretical horizontal and vertical readings are represented as green and blue lines with triangles at each sampling point.

The resampling procedure is repeated to evaluate the best possible source. Figure 9 shows particles converging after 100 iterations. The particles cumulate in the cloud of highest probability of the true source. Each particle has a different attenuation rate. The source with the smallest distance and the highest weight represents the best estimation of the true source position and attenuation parameter.

The particle filter algorithm gives not only the estimation of the best position of the source but also the best estimation of the local attenuation rate. The major advantage of the PF algorithm is that it can find a source even without correctly given parameters, which is not possible with some well-known filtering techniques such as the Kalman filter and its variants.

The cable source localization from a particle filter provided a result that complies with the diver's inspection. The difference between the calculated cable location and the location estimated by the diver is within 0.15 m, which is an error accepted by the Tinsley. Both positions are shown in the middle top sources element of Figure 9. The point estimation technique of PF will be used next to localize the section of the subsea cable.

Verification of particle filtering localization for a section of the cable

The purpose of the cable survey is to investigate a section of a cable rather than only one position as described above. The one position estimation method of particle filtering can be extended to locate the section of the cable. The MF distribution from the section of the cable on the sea surface can be sampled and measured by magnetic sensors. The sampled distribution of the MF gives an indication of the cable position. For the straight section of the cable, the only initial starting position and the initial direction can be estimated. For the particle filter algorithm, all points on the cable corresponding to the sample points are estimated along the cable section starting from the initial position and direction.

The PF algorithm for cable localization is initialized by drawing a set of hypothetical sections of the cable in the ROI. The ROI is calculated based on two peaks obtained from the horizontal and vertical searching coils. The peaks are considered on the first and last survey line.

To test the validity of the straight cable assumption, all peaks in the survey area can be regressed with linear regression. The standard goodness-of-fit test (Smith & Rose 1995) gives a good indication of the cable path.

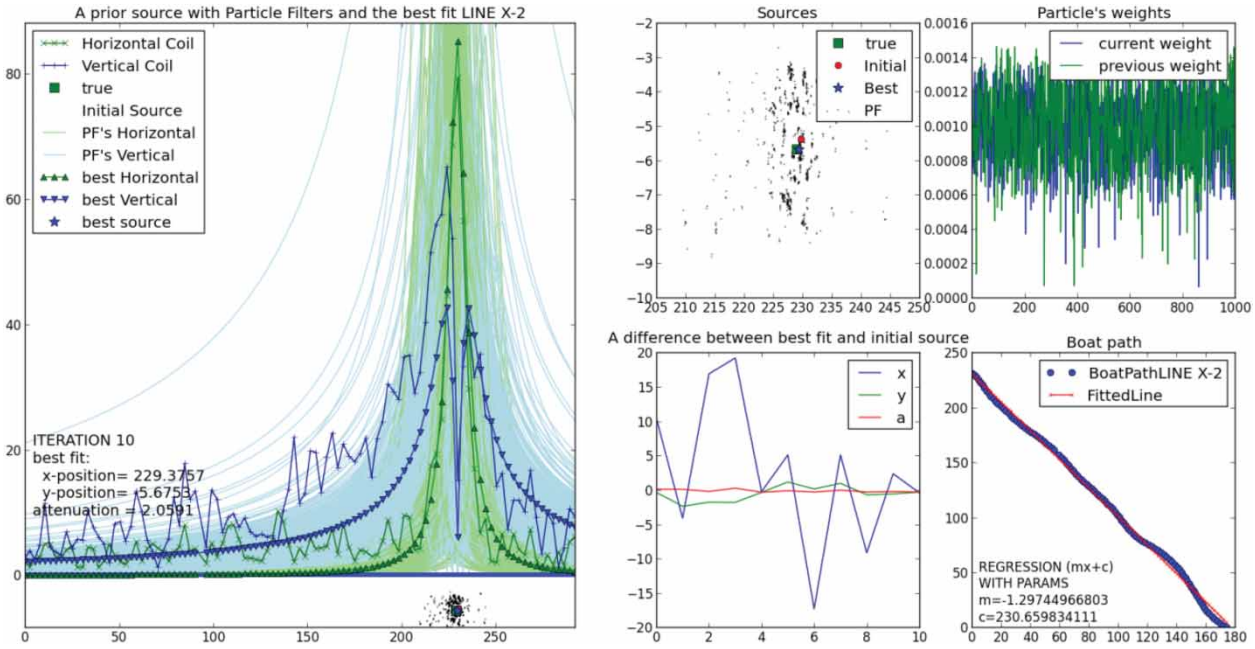

Figure 8. Particle filter after 10 iterations.

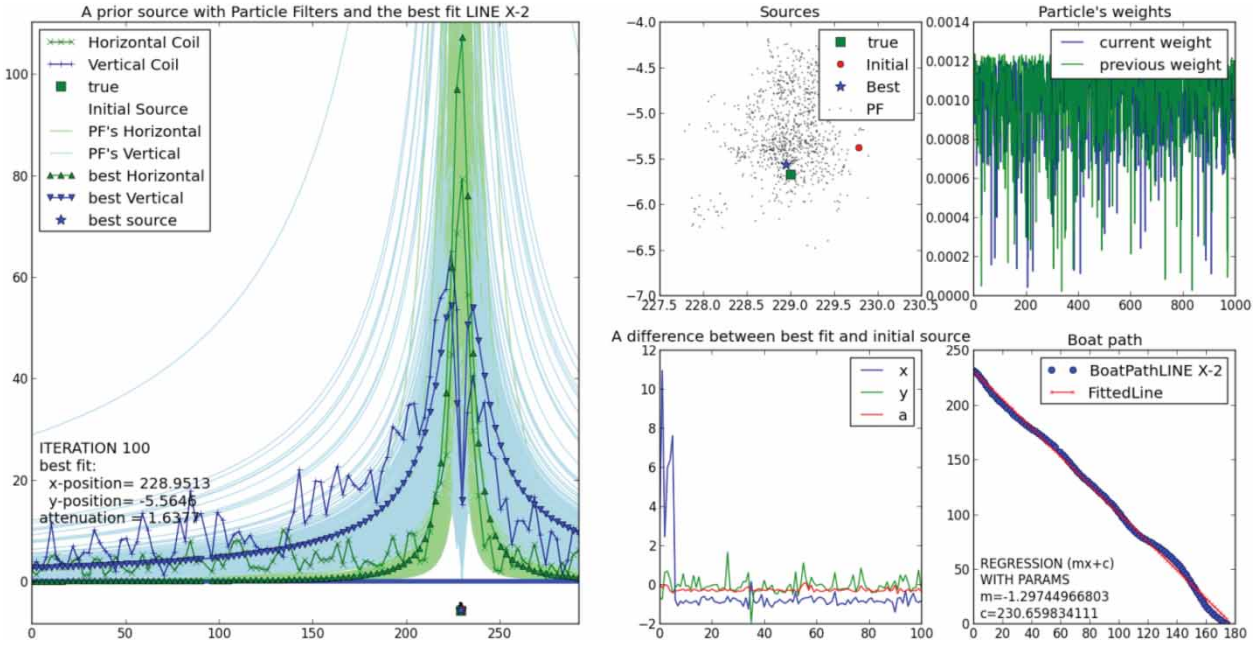

Figure 9. Particle filter after 100 iterations.

After the ROIs have been evaluated and the straight cable path assumption holds, the particle cables are drawn with starting and ending points between the ROIs. For each sample point, the nearest point on the particle cable is evaluated, and a vector of the MF is calculated using Equation (14).

Figure 10 shows the PF iteration. Ten hypothetical lines are drawn in between the ROIs region under the peaks. Each particle representing a hypothetical cable contains a possible position of the cable characterized by its directional vector and a starting-point but also includes an attenuation parameter. The particles are chosen randomly from an ROI. The distribution of MF is calculated using Equation (14), and from this value the sensors readings are calculated using Equation (16).

The algorithm becomes sensitive to the initial value of the attenuation parameter, and care should be taken to select this parameter as close as possible to its true value, taking into account prevailing environmental conditions. The particles are iterated with the initial parameters. Only

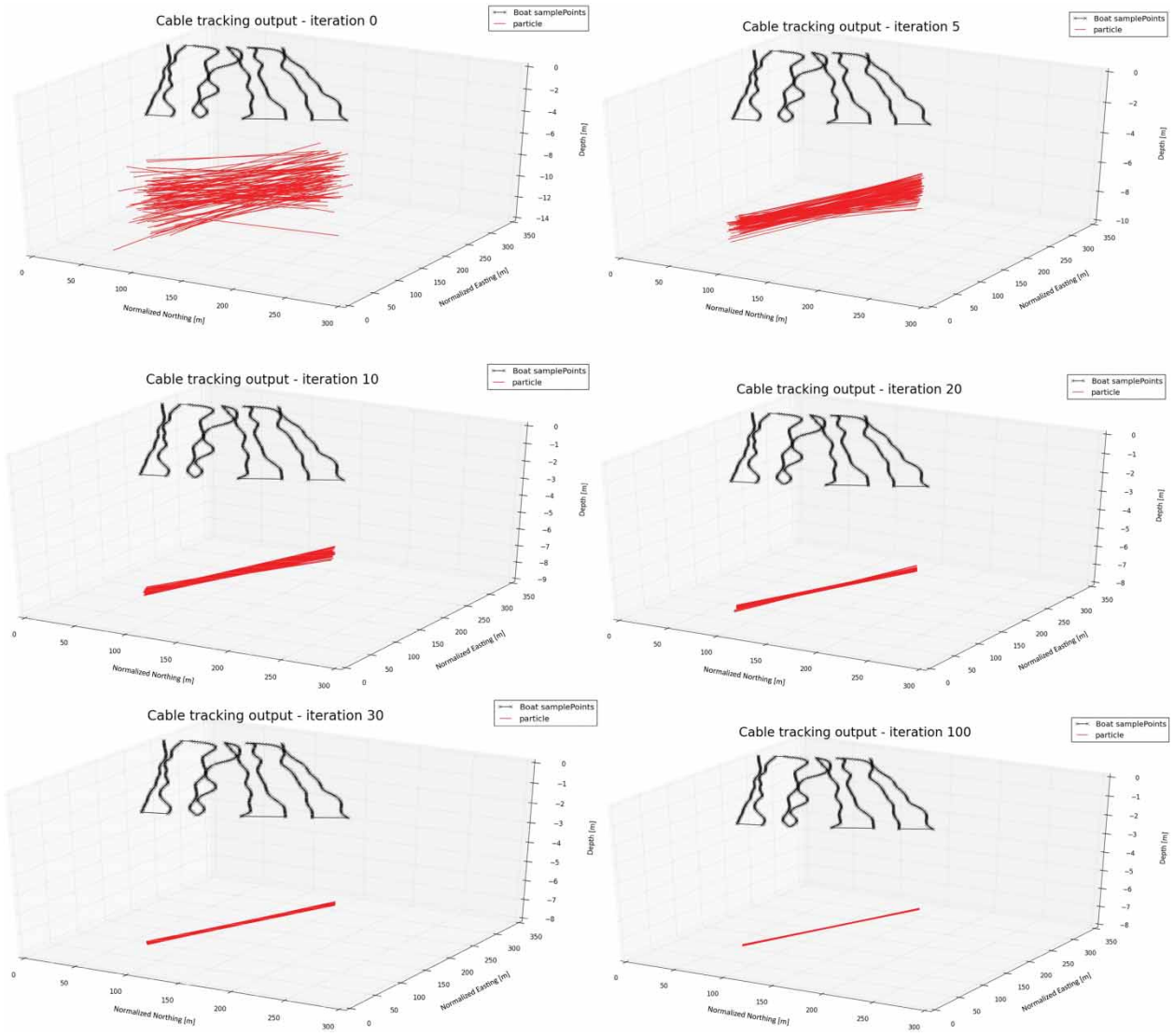

Figure 10. Particle cable iterations.

a first quartile is propagated to the next step. The distance between the particle's MF distribution and experimental data is calculated. The weights are assigned as an inverse of distances, normalized along all particles. From the set of all particles, a quarter with the highest weights are chosen to propagate to the first step. Each particle in a chosen quartile propagates with three additional particles. The additional particles cover an area close to the base particle. They are constructed based on the initial particle with added Gaussian noise. The particles move closer to the true value of the cable's location and attenuation parameter after each iteration.

It can be observed that the particles tend to cumulate in the most plausible region after five iterations. The particles converge to a small area, which is the true location of the straight section of the cable.

Point estimation and location of the straight section of the cable by PF can be used to locate any length and shape of the cable by dividing the whole section of the cable into a number of straight sections with different starting positions.

Conclusion

The subsea cable surveying is a difficult but very important task. However, the current methods based on deterministic, single sampled measurement are limited to a short distance, whereas the stochastic method of particle filters based on the whole distribution of the MF is considered an attractive alternative.

In this paper, the particle filters approach is presented, where both the starting position and the straight section of a subsea cable are localized. Particle filters correctly estimated not only the position of the cable but also the attenuation parameter, which is often difficult to obtain in a marine environment.

The method can be used on a small survey platform equipped with a magnetic sensor such as searching coils, a GPS, a heading compass and sonar to measure the water depth. Most importantly, the method eliminates the need for a diver or to engage a specialized platform such as a remotely operated or an autonomous vehicle.

Disclosure statement

No potential conflict of interest was reported by the authors.

References

Abdou AA, Shaw A, Mason A, Al-Shamma'a A, Cullen J, Wylie S. 2011. Electromagnetic (EM) wave propagation for the development of an underwater wireless sensor network (WSN). 2011 IEEE SENSORS Proc. 1:1571–1574.

Al-Shamma'a A, Shaw A, Saman S. 2004. Propagation of electromagnetic waves at MHz frequencies through seawater. IEEE Trans Antennas Propag. 52(11):2843–2849.

Bogie I. 1972. Conduction and magnetic signalling in the sea a background review. Rad Electron Eng. 42(10): 447.

Cowls S, Jordan S. 2002. The enhancement and verification of a pulse induction based buried pipe and cable survey system. OCEANS'02 MTS/IEEE. 508–511.

Crisan D, Obanubi O. 2012. Particle filters with random resampling times. Stoch Proc Appl. 122(4):1332–1368.

Dezelak K, Stumberger G, Jakl F. 2010. Arrangements of overhead power line conductors related to the electromagnetic field limits, 2010 Proceedings of the International Symposium, Wroclaw, Modern Electric Power Systems (MEPS).

El Dein AZ. 2009. Magnetic-field calculation under EHV transmission lines for more realistic cases. IEEE Trans Power Del. 24(4):2214–2222.

Fallon MF, Godsill S. 2010. Acoustic source localization and tracking using track before detect. IEEE Trans Audio, Speech, Language Process. 18(6):1228–1242.

Gard M. 2002. Magnetic field sensing in the underground construction environment. s.l., 2nd ISA/IEEE Sensors for Industry Conference. 57–65.

Gordon N. 1993. Novel approach to nonlinear/non-Gaussian Bayesian state estimation. Radar and Signal. (140): 107–113.

King RW. 1989. Lateral electromagnetic waves from a horizontal antenna for remote sensing in the ocean. IEEE Trans Antennas Propag. 37(10):1250–1255.

Kojima J, Kato Y, Asakawa K, Matumoto S, Takagi S, Kato M. 1997. Development of autonomous underwater vehicle 'AQUA EXPLORER 2' for inspection of underwater cables, MTS/IEEE Conference Proceedings, Halifax, Nova Scotia, Canada, Oceans '97.

Olsen RG, Deno D, Baishiki RS, Abbot JR, Conti R, Frazier M, Jaffa K, Niles GB, Stewart JR, Wong R, Zavadil RM. 1988. Magnetic fields from electric power lines: theory and comparison to measurements. Power Delivery, IEEE Transactions on. 3(4):2127–2136.

Olsen R, Wong P. 1992. Characteristics of low frequency electric and magnetic fields in the vicinity of electric power lines. IEEE Trans Power Del. 7(4):2046–2055.

Ortiz A, Simo M, Oliver G. 2000. Image sequence analysis for real-time underwater cable tracking. Applications of Computer Vision, 2000, Fifth IEEE Workshop on, 230–236.

Smith E, Rose K. 1995. Model goodness-of-fit analysis using regression and related techniques. Ecological Modelling. 77:49–64.

Szyrowski T, Sharma SK, Sutton R, Kennedy GA. 2013a. Developments in subsea power and telecommunication cables detection: part 1 – visual and hydroacoustic tracking. Underwater Technol. 31(3):123–132.

Szyrowski T, Sharma SK, Sutton R, Kennedy GA. 2013b. Developments in subsea power and telecommunication cables detection: part 2 – electromagnetic detection. Underwater Technol. 31(3):133–143.

Takagi S, Kojima J, Asakawa K. 1996. DC cable sensors for locating underwater telecommunication cables. OCEANS 96 MTS/IEEE Conference Proceedings. The Coastal Ocean – Prospects for the 21st Century, 339–344.

Tinsley. 2012. Tinsley.co.uk. [En ligne] Available from: http://tinsley.co.uk/index.htm [Accessed 1st November 2013].

Tumanski S. 2007. Induction coil sensors – a review. Meas Sci Technol. 18(3):R31–R46.

Won I. 2003. Characterization of UXO-like targets using broadband electromagnetic induction sensors. IEEE Trans Geosci Remote. 41(3):652–663.